Nematic Spin Correlations Pervading the Phase Diagram of FeSe$_{1-x}$S$_x$

Ruixian Liu,[1] Wenliang Zhang👤,[2] Yuan Wei,[2] Zhen Tao,[1,2] Teguh C. Asmara,[2,3] Yi Li,[1] Vladimir N. Strocov,[2]
Rong Yu,[4] Qimiao Si,[5] Thorsten Schmitt,[2,*] and Xingye Lu👤[1,†]

[1]*Center for Advanced Quantum Studies and Department of Physics, Beijing Normal University,*
Beijing 100875, People's Republic of China
[2]*Photon Science Division, Swiss Light Source, Paul Scherrer Institut, CH-5232 Villigen PSI, Switzerland*
[3]*European X-Ray Free-Electron Laser Facility GmbH, 22869 Schenefeld, Germany*
[4]*Department of Physics, Renmin University of China, Beijing 100872, China*
[5]*Department of Physics and Astronomy, Rice Center for Quantum Materials, Rice University, Houston, Texas 77005, USA*

We use resonant inelastic x-ray scattering (RIXS) at the Fe-L$_3$ edge to study the spin excitations of uniaxial-strained and unstrained FeSe$_{1-x}$S$_x$ ($0 \leq x \leq 0.21$) samples. The measurements on unstrained samples reveal dispersive spin excitations in all doping levels, which show only minor doping dependence in energy dispersion, lifetime, and intensity, indicating that high-energy spin excitations are only marginally affected by sulfur doping. RIXS measurements on uniaxial-strained samples reveal that the high-energy spin-excitation anisotropy observed previously in FeSe is also present in the doping range $0 < x \leq 0.21$ of FeSe$_{1-x}$S$_x$. The spin-excitation anisotropy persists to a high temperature up to $T > 200$ K in $x = 0.18$ and reaches a maximum around the nematic quantum critical doping ($x_c \approx 0.17$). Since the spin-excitation anisotropy directly reflects the existence of nematic spin correlations, our results indicate that high-energy nematic spin correlations pervade the regime of nematicity in the phase diagram and are enhanced by the nematic quantum criticality. These results emphasize the essential role of spin fluctuations in driving electronic nematicity and highlight the capability of uniaxial strain in tuning spin excitations in quantum materials hosting strong magnetoelastic coupling and electronic nematicity.

Nematic order in quantum materials refers to an electronic state characterized by broken rotational symmetry and retained orientational order (or translational symmetry) [1]. In iron-based superconductors (FeSCs), nematic order manifests as strong in-plane C_2 symmetric electronic anisotropies in the paramagnetic orthorhombic state [2–13]. Under uniaxial strain (ε) along the a/b axis, such an anisotropy can persist to a temperature range beyond the nematic transition, revealing the fluctuating regime in the tetragonal state [4,5,8–13]. Since electronic nematicity is essential for determining the exotic electronic properties of FeSCs and driving other emergent orders therein, it has attracted tremendous research interest in the past decade [2–5,7].

FeSe$_{1-x}$S$_x$, hosting exotic electronic properties and a pristine nematic transition without subsequent magnetic transition has been a focus of studying electronic nematicity and its correlation with other intertwined order and fluctuations [4,7,14,15]. The parent compound FeSe exhibits a tetragonal-to-orthorhombic structural (nematic) transition at $T_s \approx 90$ K and a superconducting transition at $T_c \approx 8$ K [Fig. 1(a)] [16,17]. The nematic state at $T < T_s$ is a quantum-disordered magnetic state with intense antiferromagnetic (AF) spin excitations [18–23]. With increasing sulfur doping, the nematic transition is gradually suppressed to $T_s = 0$ at the putative nematic quantum critical

point (NQCP) ($x_c \approx 0.17$), while T_c increases slightly from $T_c \approx 8$ K ($x = 0$) to $T_c \approx 10$ K ($x \approx 0.08$) and decreases to $T_c \approx 5$ K across the NQCP [7].

Beyond the nematic ordering region at $T \leq T_s$ and $x \leq x_c$, static nematic susceptibility (χ_{nem}) of FeSe$_{1-x}$S$_x$ derived from elastoresistance measurements revealed a widely spread nematic fluctuating regime in the tetragonal phase ($T > T_s$ and $x > x_c$) [24]. The NQCP leads to maximized χ_{nem} [24] and induces dramatic changes in various electronic properties [4,25–27]. Although the static $\chi_{\text{nem}}(T)$ demonstrated that the nematicity is electronic in origin [10] and revealed the nematic fluctuating regime in FeSe$_{1-x}$S$_x$ [24], it cannot distinguish which degree of freedom (spin, orbital, charge) plays a dominant role in driving the electronic nematicity.

In our prior RIXS study of detwinned FeSe, the high-energy spin-excitation anisotropy along the H/K axes observed in the nematic state has been used to characterize the nematic spin correlations—the manifestation of electronic nematicity in the spin (fluctuation) channel [28]. The anisotropy can persist to a temperature slightly above T_s and suggests that the electronic nematicity in FeSe is spin driven. Alternatively, x-ray absorption dichroism measurements of FeSe revealed that orbital polarization under fixed strain exhibited a Curie-Weiss behavior in the fluctuating regime

and suggested an orbital origin of the nematicity [29]. To obtain more insights into understanding the electronic nematicity, it is important to explore how the AF spin excitation and the anisotropy evolve across the nematic regime in $FeSe_{1-x}S_x$. In particular, upon sulfur doping, as the nematic order weakens and disappears at the NQCP, it remains unknown to what extent the nematic spin correlations will pervade the phase diagram and be affected by the NQCP.

To address these issues, we use Fe-L_3 RIXS to measure the spin excitations of unstrained and uniaxial-strained $FeSe_{1-x}S_x$ ($x = 0$–0.21) across the NQCP [Fig. 1(a)] [30–33]. To explore the nematic spin correlations, one needs to apply uniaxial strain along the a/b axis of $FeSe_{1-x}S_x$ and measure the possible spin-excitation anisotropy [28]. In this work, we use a uniaxial strain device based on differential thermal expansions of invar alloy and aluminum to apply uniaxial strain on $FeSe_{1-x}S_x$ [Fig. 1(b)] [34,35]. While the measurements on unstrained samples reveal persistent spin excitations with minor doping dependence (Figs. 2 and 3), the measurements on uniaxial-strained samples reveal an enhancement of the spin-excitation anisotropy near the NQCP. Moreover, the prominent spin-excitation anisotropy persists for high doping levels ($x = 0.21$) and temperature ($T > 100$ K in $x = 0.11$ and $T > 200$ K in $x = 0.18$) far beyond the nematic ordering region, demonstrating that the high-energy nematic spin correlations pervade a wide doping and temperature range in the phase diagram of $FeSe_{1-x}S_x$. Our results demonstrate that the regime of nematic ordering and nematic quantum criticality (NQC) is preceded by nematic spin fluctuations that dominate the nematic fluctuating regime. This discovery corroborates the spin-nematic picture and provides new insight for understanding the interplay between the intertwined orders and fluctuations in $FeSe_{1-x}S_x$.

The doping levels studied in this work are marked by vertical red bars in the phase diagram of $FeSe_{1-x}S_x$ [Fig. 1(a)]. Figure 1(b) illustrates the scattering geometry and the reciprocal space of the RIXS measurements, which were performed near the Fe-L_3 edge (incident energy $E_i \approx 708$ eV) as shown in the total fluorescence yield (TFY) x-ray absorption spectroscopy (XAS) data in Fig. 1(c). The RIXS and XAS measurements were carried out with the RIXS experimental station at the ADRESS beamline of the Swiss Light Source at the Paul Scherrer Institut [35,39,40].

To apply uniaxial strain on the sample, a thin $FeSe_{1-x}S_x$ crystal was glued onto the titanium bridge in the center of the uniaxial-strain device using epoxy [Fig. 1(b)]. Upon cooling, the differential thermal expansion coefficients between the aluminum frame ($\alpha \approx -24 \times 10^{-6}$/K) and the invar-alloy blocks ($\alpha \approx -2 \times 10^{-6}$/K) can generate a uniaxial strain up to $\varepsilon = \varepsilon_{xx} - \varepsilon_{yy} \approx -0.8\%$ on the neck of the titanium bridge at low temperature, which can be
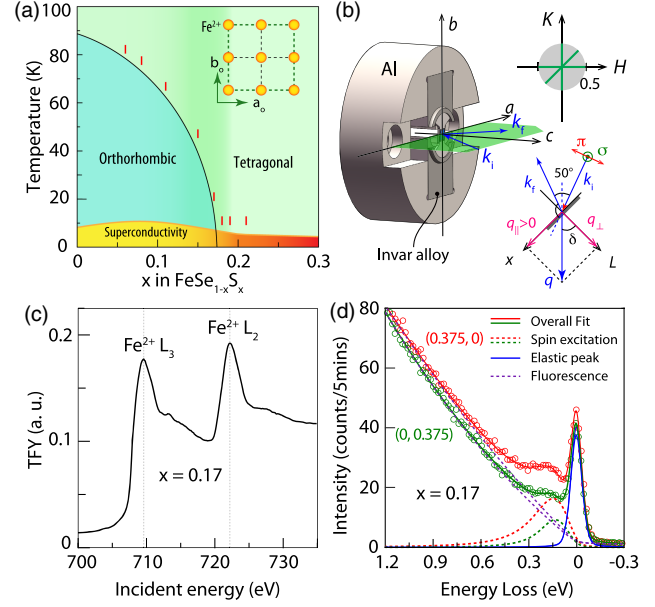

FIG. 1. (a) Electronic phase diagram of $FeSe_{1-x}S_x$. The red vertical bars mark the doping levels measured in the present study. (b) Schematics of scattering geometry with a crystal glued on a uniaxial strain device. The scattering angle was set to $2\theta_s = 130°$. (c) Total fluorescence yield (TFY) x-ray absorption spectroscopy data of $FeSe_{1-x}S_x$ ($x = 0.17$). (d) RIXS spectra of a uniaxial-strained $x = 0.17$ sample measured at $\mathbf{q}_\parallel = (0.375, 0)$ and $(0, 0.375)$, $T = 20$ K. The red and green solid curves are the overall fittings of the spectra. The red and green dashed curves are fittings of the spin excitations. The magenta dashed curves and the blue solid curves describe the fluorescence tail and the elastic peaks, respectively.

transferred to the thin crystal glued on it [34,35]. The uniaxial strain on the sample's surface can be accurately measured using a microscope [35].

To facilitate the discussion of the results presented below, we denote the RIXS spectra and the spin excitations along H, K and $[H, H]$ directions as $I_{h/k/hh}(q_\parallel, E)$ and $S_{h/k/hh}(q_\parallel, E)$, respectively. The RIXS spectrum $I(q_\parallel, E)$ consists of fluorescence $I_{\text{fluo}}(E)$, an elastic peak $I_{\text{el}}(E)$, and $S(q_\parallel, E)$. Figure 1(d) shows two representative RIXS spectra $I_h(q_\parallel, E)$ (red circles) and $I_k(q_\parallel, E)$ (green circles) ($q_\parallel = 0.375$) of an $x = 0.17$ sample measured under a uniaxial strain of $\varepsilon \approx -0.6\%$ (at $T = 20$ K) along the b axis. Because the spin excitations of twined or unstrained FeSC crystals would be C_4 symmetric [$I_h(q_\parallel, E) = I_k(q_\parallel, E)$], the substantial difference between $I_h(q_\parallel, E)$ and $I_k(q_\parallel, E)$ clearly reveals an excitation anisotropy induced by the uniaxial strain. The fitting analysis of the spectra agrees well with the raw data (red and green circles) [35] and reveals a strong anisotropy between $S_h(q_\parallel, E)$ (red dashed curve) and $S_k(q_\parallel, E)$ (green dashed curve), unveiling the existence of nematic spin correlations in $FeSe_{1-x}S_x$.

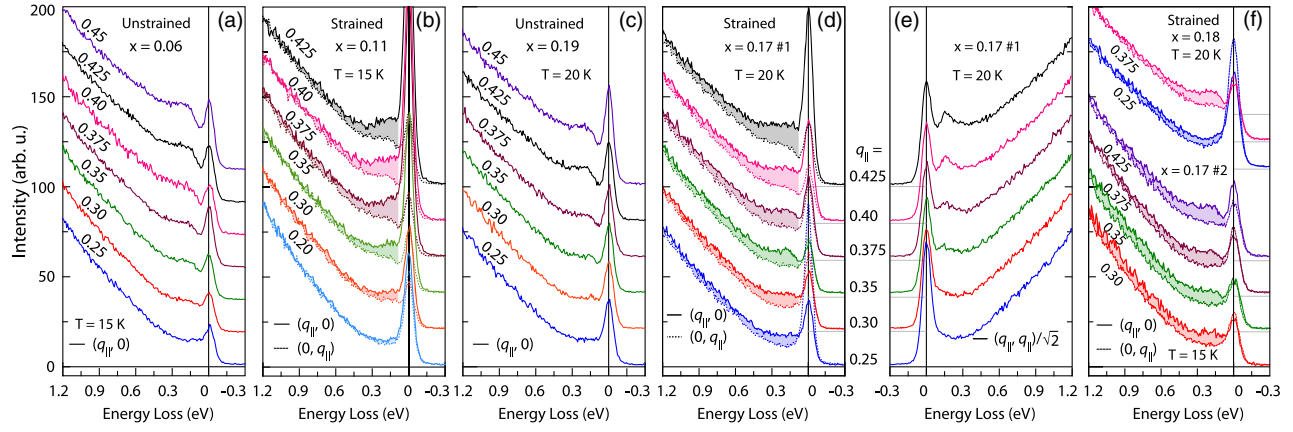Having established the experimental strategy, we have carried out systematic RIXS measurements on unstrained

FIG. 2.   (a),(c) $q_{\parallel}$-dependent RIXS spectra along H direction of unstrained $x = 0.06$ and 0.19 samples. (b) RIXS spectra along H (solid curves) and K (dashed curves) directions of uniaxial-strained $x = 0.11$ sample. (d),(e) RIXS spectra measured along (d) H/K and (e) $[H, H]$ directions of uniaxial-strained $x = 0.17$ sample 1. (f) RIXS spectra along H/K directions of uniaxial-strained $x = 0.17$ (sample 2) and 0.18. The color shaded areas mark the difference between $I_h(q_{\parallel})$ and $I_k(q_{\parallel})$.

and uniaxial-strained FeSe$_{1-x}$S$_x$ samples in the doping range $x = 0.06$–0.21 to sort out the development of the spin excitations and their anisotropy (Figs. 2–4) across the electronic phase diagram. Figure 2 displays the momentum-dependent RIXS spectra measured at $T = 15$ and 20 K on unstrained $x = 0.06$ [Fig. 2(a)], strained $x = 0.11$ [$\varepsilon \approx -0.8\%$ Fig. 2(b)], unstrained $x = 0.19$ [Fig. 2(c)], strained $x = 0.17$ (sample 1) [$\varepsilon \approx -0.6\%$, Figs. 2(d) and 2(e)], and strained $x = 0.18$ [$\varepsilon \approx -0.4\%$, Fig. 2(f)], and the $x = 0.17$ (sample 2) [$\varepsilon \approx -0.6\%$, Fig. 2(f)] samples in which $x = 0.06$ and 0.11 are in the nematic ordering regime, $x = 0.17$ at the NQCP, and $x = 0.18$ and 0.19 in the tetragonal phase [35]. All spectra were normalized according to the doping-independent fluorescence in the energy-loss range of [1, 10] eV. The waterfall plots in Fig. 2 show that dispersive spin excitations along the H/K and $[H, H]$ directions are observed in a wide doping range covering the nematic regime. For the unstrained samples, the momentum-dependent RIXS spectra of $x = 0.19$ are similar to those of the $x = 0.06$ ($T_s \approx 74$ K) sample, implying only a subtle change of the spin excitations across the phase boundary of the nematic order. For the strained samples, the RIXS spectra collected both in the nematic ordering regime ($x = 0.11$, $T_s \approx 65$ K), and close to the NQCP ($x = 0.17$ and 0.18 samples), exhibit prominent excitation anisotropy [$I_h(q_{\parallel}, E) > I_k(q_{\parallel}, E)$] in Fig. 2.

To extract the information of the spin excitations and understand the spin-excitation anisotropy quantitatively, we use the damped harmonic oscillator (DHO) function to describe the spin excitations $S(q, E) = A \cdot 2\gamma E / [(E^2 - E_0^2)^2 + (\gamma E)^2]$ [20,28], where $E_0(\mathbf{q}_{\parallel})$ is the undamped energy and $\gamma(\mathbf{q}_{\parallel})$ is the damping factor. The undamped energy $E_0(\mathbf{q}_{\parallel})$ and the excitation lifetime $\gamma(\mathbf{q}_{\parallel})$ in the DHO formula characterize the line shape of the excitations. If $E_0 > \gamma/2$ ($E_0 < \gamma/2$), the spin excitations are underdamped (overdamped).

Figure 3 summarizes the fitting results of the RIXS spectra collected in the doping range covering the nematic phase and the NQCP ($x_c \approx 0.17$). Figure 3(a) shows the energy dispersion $E_0(\mathbf{q}_{\parallel})$ (colored symbols) and the damping rate $\gamma/2$ (colored lines) for the spin excitations of unstrained samples, for which the unstrained $I_h(q_{\parallel}, E)$ of $x = 0.11$ and 0.17 were obtained by averaging the $I_h(q_{\parallel}, E)$ and $I_k(q_{\parallel}, E)$ of uniaxial-strained samples. The energy dispersion $E_0(\mathbf{q}_{\parallel})$ exhibits negligible doping dependence along both $[H, 0]$ and $[H, H]$ directions. Moreover, the damping rate $\gamma/2$ also shows a minor doping dependence. As $\gamma/2$ is overall lower than E_0 in the whole momentum range studied, all the spin excitations observed here are underdamped paramagnons. The doping dependence of E_0 and $\gamma/2$ indicates that the high-energy spin excitations are not affected by sulfur doping. This is further evidenced by the doping-independent E_0 and $\gamma/2$ [Fig. 3(b)], and the largely unchanged energy-integrated intensity $S_h(q_{\parallel})$ [red diamonds in Fig. 3(c)] for $\mathbf{q}_{\parallel} = (0.375, 0)$ for all dopings. For $S_h(q_{\parallel} = 0.375)$, E_0 is constantly larger than $\gamma/2$, consistent with underdamped spin-excitation modes. Figure 3(c) shows the energy- and $q_{\parallel}$-integrated (within the momentum interval $q_{\parallel} = [0.25, 0.425]$) intensity of the spin excitations along the H axis of unstrained samples (black filled circles). Again, the integrated spectral weight remains unchanged from $x = 0$ to 0.19.

Figure 3(d) exhibits the undamped energy dispersion $E_0(\mathbf{q}_{\parallel})$ of $S_h(q_{\parallel}, E)$ and $S_k(q_{\parallel}, E)$ for uniaxial-strain detwinned $x = 0$ and 0.11 ($T_s \approx 65$ K). The $E_0(\mathbf{q}_{\parallel})$ along H and K directions overlap for these two dopings. In comparison, $S_h(q_{\parallel}, E)$ and $S_k(q_{\parallel}, E)$ in $x = 0.17$ exhibit a clear difference in $E_0(\mathbf{q}_{\parallel})$ [Fig. 3(e)], indicating that the uniaxial strain can induce a pronounced difference in the energy dispersion of spin excitations near the NQCP. Figure 3(f) displays the energy-integrated intensity of the spin excitations $S_h(q_{\parallel})$ and $S_k(q_{\parallel})$ for $x = 0.11$ and 0.17,
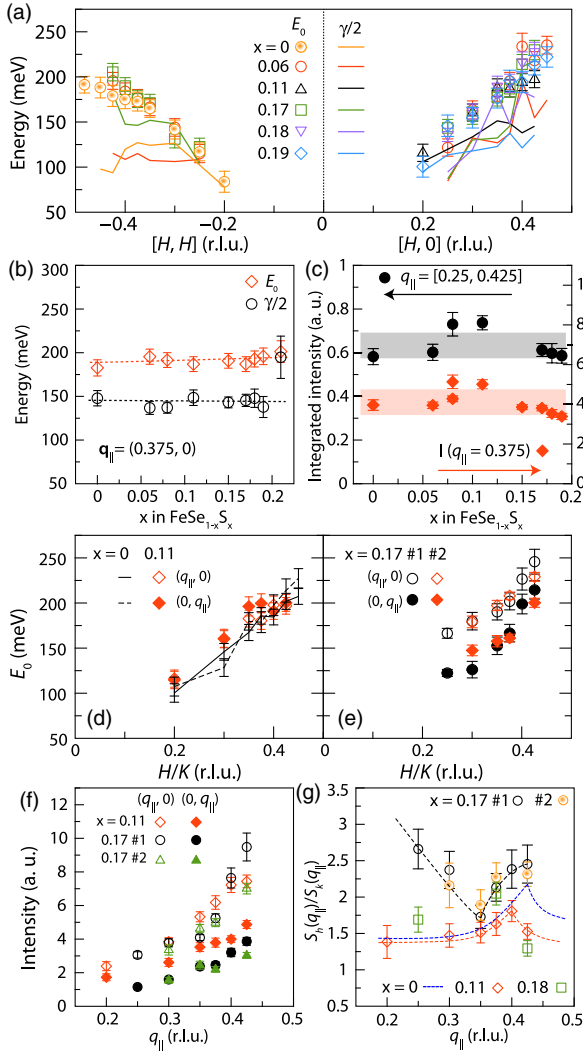
FIG. 3. (a) E_0 and $\gamma/2$ of the spin excitations along H $[S_h(q_\parallel, E)]$ and $[H, H]$ $[S_{hh}(q_\parallel, E)]$ for unstrained $x = 0, 0.06,$ $0.11, 0.17, 0.18,$ and 0.19. (b) E_0 and $\gamma/2$ of the spin excitation at $H = 0.375$ of unstrained samples as a function of the doping level x. (c) Doping dependence of the spin-excitation intensity $S_h(q_\parallel)$ for $q_\parallel = 0.375$ (red diamonds) and the momentum integrated $S_h(q_\parallel)$ in the momentum range $q_\parallel = [0.25, 0.425]$ (black circles). (d),(e) Comparison of $E_0(q_\parallel)$ between $S_h(q_\parallel, E)$ and $S_k(q_\parallel, E)$ for (d) $x = 0$ (black lines), 0.11 (red diamonds), and (e) $x = 0.17$. (f) Energy-integrated spin-excitation intensity $S_h(q_\parallel)$ (open symbols) and $S_k(q_\parallel)$ (filled symbols) for $x = 0.11$ (red diamonds), 0.17 (sample 1) (black circles), and 0.17 (sample 2) (green triangles). (g) Doping-dependent spin-excitation anisotropy $\phi(q_\parallel) = S_h(q_\parallel)/S_k(q_\parallel)$ for $x = 0$ (blue dashed curve), 0.11 (red diamonds), 0.17 (black and illuminated orange circles), and 0.18 (green squares). The red and black dashed curves are guides to the eyes.

from which we determine the magnitude of the spin-excitation anisotropy as $\phi(q_\parallel) = S_h(q_\parallel)/S_k(q_\parallel)$ [Fig. 3(g)]. The anisotropy in $x = 0.11$ is overall slightly lower than that of FeSe (blue dashed curve), indicating that the intrinsic nematic spin correlations in the nematic state

weaken as the sulfur doping increases, which suppresses the nematic transition.

With further increase of doping, the nematic order is completely suppressed at $x = 0.17$; i.e., this doping creates a tetragonal system at finite temperature. Surprisingly, RIXS measurements on $x = 0.17$ with $\varepsilon \approx -0.6\%$ reveal a pronounced spin-excitation anisotropy that is even stronger than those in detwinned FeSe ($\varepsilon \approx -0.54\%$ at $T = 20$ K) and FeSe$_{0.89}$S$_{0.11}$ ($\varepsilon \approx -0.8\%$ at $T = 15$ K) [Fig. 3(g)]. Since the $x = 0.17$ sample falls in the regime of NQC, the enhancement of the nematic spin correlations could be driven by strong nematic fluctuations near the NQCP [41].

To further assess the enhancement of nematic spin correlations near the NQCP and illustrate the nematic spin correlations in the fluctuating regime, we show in Fig. 4 the temperature and doping dependence of the spin-excitation anisotropy $\phi(q_\parallel)$ at $q_\parallel = 0.375$. We find that the anisotropy at $T = 15$ K in $x = 0.11$ decreases only by $\sim 15\%$ when warmed to $T = 100$ K ($> T_s = 65$ K) [inset of Fig. 4(a)], indicating that the nematic spin correlations can persist to higher temperatures well above T_s in the nematic ordering regime ($x < x_c$). Furthermore, we show in Fig. 4(a) $I_h(q_\parallel, E)$ and $I_k(q_\parallel, E)$ of $x = 0.18$ (slightly higher than x_c) measured under a moderate uniaxial strain $\varepsilon \approx -0.4\%$ ($T = 20$ K). The spectra show clear difference at $T = 20$ K, generating $\phi(q_\parallel) \approx 1.8$ [inset of Fig. 4(a)]. Upon warming, while the uniaxial strain was relaxed gradually, the anisotropy, however, persists at $T = 200$ K (decreased by $\sim 40\%$) and finally vanishes at $T = 320$ K [Fig. 4(a)].

Figure 4(b) shows the spectra $I_h(q_\parallel, E)$ and $I_k(q_\parallel, E)$ measured at the same $q_\parallel = 0.375$ near the regime of NQC. Similar spectral difference is observed in $x = 0.15$ ($T_s = 50$ K, $\varepsilon \approx -0.6\%$) and $x = 0.21$ ($\varepsilon \approx -0.4\%$) at $T = 20$ K [color shaded areas in Fig. 4(b)]. The inset of Fig. 4(b) depicts the doping dependence of the spin-excitation anisotropy $I_h(q_\parallel, E)/I_k(q_\parallel, E)$ for $x = 0.15$ ($\varepsilon \approx -0.6\%$, blue), $x = 0.17$ ($\varepsilon \approx -0.6\%$, red), $x = 0.18$ ($\varepsilon \approx -0.4\%$, green), and $x = 0.21$ ($\varepsilon \approx -0.4\%$, black), revealing a decreasing tendency for higher doping. We note that the anisotropy of the RIXS spectra persists to an energy scale ~ 1 eV of the electron-hole pair tail, which could be attributed to an anisotropy in incoherent charge scattering [42].

Figure 4(c) summarizes the doping-dependent spin-excitation anisotropy $\phi(q_\parallel)$ with $q_\parallel = 0.375$ extracted from the fitting of the spin excitations [35]. Consistent with the enhancement at $x = 0.17$ [Fig. 3(g)], the anisotropy in Fig. 4(c) reaches a maximum in the doping region $x \approx 0.15$–0.18. Such a doping dependence of the nematic spin fluctuations [nematic spin susceptibility $\chi''(\mathbf{q}_\parallel, E)$] is much akin to the static χ_{nem} reported in Ref. [24]. This is solid evidence of the spin-nematic picture [24]. It is well known that quantum critical fluctuations usually dominate
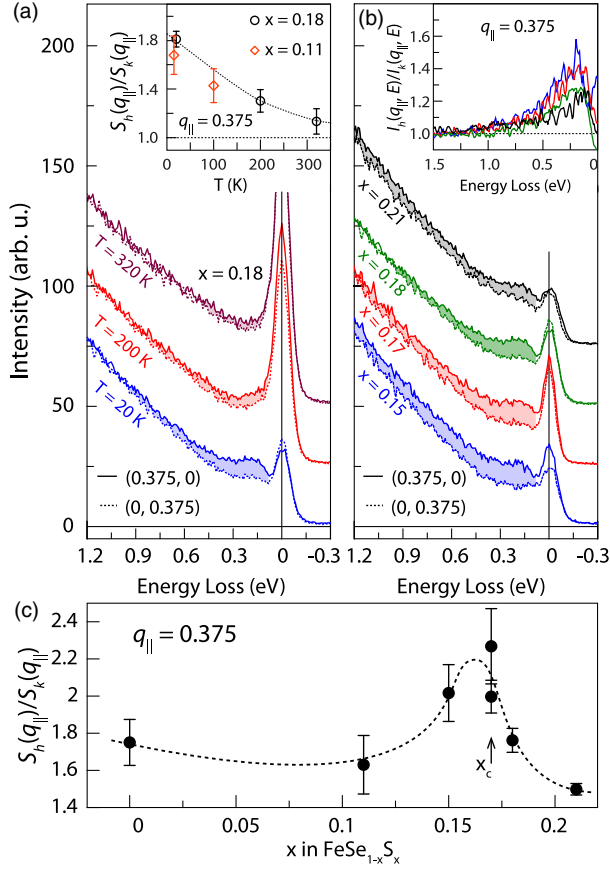
FIG. 4. Temperature and doping dependence of the spin-excitation anisotropy of uniaxial-strained $FeSe_{1-x}S_x$. (a) Temperature dependence of the RIXS spectra for $\mathbf{q}_{\parallel} = (0.375, 0)$ and $(0, 0.375)$ for $x = 0.18$ measured at $T = 20$, 200, and 320 K with $\varepsilon \approx -0.6\%$ at $T = 20$ K. The inset shows the temperature-dependent intensity ratio $\phi(q_{\parallel}) = S_h(q_{\parallel})/S_k(q_{\parallel})$ with $q_{\parallel} = 0.375$ for $x = 0.11$ and 0.18. $\phi(q_{\parallel})$ are obtained from the fitting of the spin excitations. (b) Doping-dependent RIXS spectra ($x = 0.15$, 0.17, 0.18, and 0.21) with $\mathbf{q}_{\parallel} = (0.375, 0)$ and $(0, 0.375)$. The colored areas mark the difference between the spectra $I_h(q_{\parallel})$ and $I_k(q_{\parallel})$. The inset shows the ratio between $I_h(q_{\parallel})$ and $I_k(q_{\parallel})$ for $x = 0.15$, 0.17 (sample 1), 0.18, and 0.21. (c) Doping dependence of the $\phi(q_{\parallel})$ with $q_{\parallel} = 0.375$.

static electronic transport properties and low-energy charge or spin dynamics [43]. The $E \sim 200$ meV nematic spin correlations exhibiting a maximum near the NQCP strongly suggest that the nematic fluctuation can also dominate the spin dynamics at a much higher energy scale.

The nematic fluctuating regime in FeSCs has been well established in various studies of (quasi)static properties, such as the softening of the shear modulus C_{66} [44–46], the divergent nematic susceptibility obtained from elastoresistance $-2m_{66}$ [11,24], and the persistence of local orthorhombicity (short-range orthorhombic structure) in the tetragonal state of both iron pnictides and FeSe [38,47–49]. As such a local orthorhombicity persists in both iron pnictides and iron chalcogenides, it should be a common

feature of the nematic fluctuating regime of FeSCs. Our identification of spin-excitation anisotropy at high energies is consistent with the general notion that high-energy fluctuations are concomitant with short-range spatial correlations. Our results thus uncover a common feature that high-energy nematic spin fluctuations permeate across FeSCs.

It is important to note that our result is to some extent compatible with the orbital polarization result in Ref. [29] as low-energy nematic spin correlations could arise from orbital selective Fermi surface nesting [50,51]. It is also not against some work emphasizing the fundamental role of electron correlations across the nematic regime [52], though it remains an open question how to reconcile all the diverse experimental discoveries supporting different scenarios within one theoretical frame.

In summary, we find the high-energy spin-excitations in $FeSe_{1-x}S_x$ ($x \lesssim 0.21$) are only marginally affected by sulfur doping, and illustrate that the nematic spin correlations pervade a wide doping ($0 \lesssim x \lesssim 0.21$) and temperature region of the phase diagram. As the nematic spin correlations precede the nematic ordering regime and exhibit an enhancement near the NQCP, it could be the origin of the nematic fluctuations, thus corroborating the spin-nematic picture. The strain-induced spin-excitation anisotropy in the tetragonal state of $FeSe_{1-x}S_x$ highlights the capability of uniaxial strain in tuning spin and/or charge fluctuations in similar quantum materials hosting electron-lattice coupling.

*thorsten.schmitt@psi.ch
†luxy@bnu.edu.cn

[1] E. Fradkin, S. A. Kivelson, and J. M. Tranquada, Colloquium: Theory of intertwined orders in high temperature superconductors, Rev. Mod. Phys. **87**, 457 (2015).

[2] R. M. Fernandes, A. V. Chubukov, and J. Schmalian, What drives nematic order in iron-based superconductors?, Nat. Phys. **10**, 97 (2014).

[3] Q. Si, R. Yu, and E. Abrahams, High temperature superconductivity in iron pnictides and chalcogenides, Nat. Rev. Mater. **1**, 16017 (2016).

[4] Q. Si and N. E. Hussey, Iron-based superconductors: Teenage, complex, challenging, Phys. Today **76**, No. 5, 34 (2023).

[5] R. M. Fernandes *et al.*, Iron pnictides and chalcogenides: A new paradigm for superconductivity, Nature (London) **601**, 39 (2022).

[6] A. Böhmer, J.-H. Chu, S. Lederer, and M. Yi, Nematicity and nematic fluctuations in iron-based superconductors, Nat. Phys. **18**, 1412 (2022).

[7] A. I. Coldea, Electronic nematic states tuned by isoelectronic substitution in bulk $FeSe_{1-x}S_x$, Front. Phys. **8**, 594500 (2021).

[8] J.-H. Chu, J. G. Analytis, K. De Greve, P. L. McMahon, Z. Islam, Y. Yamamoto, and I. R. Fisher, In-plane resistivity anisotropy in an underdoped iron arsenide superconductor, Science **329**, 824 (2010).

[9] M. Yi *et al.*, Symmetry-breaking orbital anisotropy observed for detwinned $Ba(Fe_{1-x}Co_x)_2As_2$ above the spin density wave transition, Proc. Natl. Acad. Sci. U.S.A. **108**, 6878 (2011).

[10] J.-H. Chu, H.-H. Kuo, J. G. Analytis, and I. R. Fisher, Divergent nematic susceptibility in an iron arsenide superconductor, Science **337**, 710 (2012).

[11] H.-H. Kuo, J.-H. Chu, J. C. Palmstrom, S. A. Kivelson, and I. R. Fisher, Ubiquitous signatures of nematic quantum criticality in optimally doped Fe-based superconductors, Science **352**, 958 (2016).

[12] X. Lu, J. T. Park, R. Zhang, H. Luo, A. H. Nevidomskyy, Q. Si, and P. Dai, Nematic spin correlations in the tetragonal state of uniaxial-strained $BaFe_{2-x}Ni_xAs_2$, Science **345**, 657 (2014).

[13] X. Lu *et al.*, Spin waves in detwinned $BaFe_2As_2$, Phys. Rev. Lett. **121**, 067002 (2018).

[14] A. Coldea and M. D. Watson, The key ingredients of the electronic structure of FeSe, Annu. Rev. Condens. Matter Phys. **9**, 125 (2018).

[15] T. Shibauchi, T. Hanaguri, and Y. Matsuda, Exotic superconducting states in FeSe-based materials, J. Phys. Soc. Jpn. **89**, 102002 (2020).

[16] F. C. Hsu *et al.*, Superconductivity in the PbO-type structure α-FeSe, Proc. Natl. Acad. Sci. U.S.A. **105**, 14262 (2008).

[17] T. M. McQueen, A. J. Williams, P. W. Stephens, J. Tao, Y. Zhu, V. Ksenofontov, F. Casper, C. Felser, and R. J. Cava, Tetragonal-to-orthorhombic structural phase transition at 90K in the superconductor $Fe_{1.01}Se$, Phys. Rev. Lett. **103**, 057002 (2009).

[18] Q. Wang *et al.*, Strong interplay between stripe spin fluctuations, nematicity and superconductivity in FeSe, Nat. Mater. **15**, 159 (2016).

[19] Q. Wang *et al.*, Magnetic ground state of FeSe, Nat. Commun. **7**, 12182 (2016).

[20] M. C. Rahn, K. Kummer, N. B. Brookes, A. A. Haghighirad, K. Gilmore, and A. T. Boothroyd, Paramagnon dispersion in β-FeSe observed by Fe L-edge resonant inelastic x-ray scattering, Phys. Rev. B **99**, 014505 (2019).

[21] J. Pelliciari *et al.*, Evolution of spin excitations from bulk to monolayer FeSe, Nat. Commun. **12**, 3122 (2021).

[22] F. Wang, S. Kivelson, and D.-H. Lee, Nematicity and quantum paramagnetism in FeSe, Nat. Phys. **11**, 959 (2015).

[23] R. Yu and Q. Si, Antiferroquadrupolar and Ising-nematic orders of a frustrated bilinear-biquadratic Heisenberg model and implications for the magnetism of FeSe, Phys. Rev. Lett. **115**, 116401 (2015).

[24] S. Hosoi, K. Matsuura, K. Ishida, H. Wang, Y. Mizukami, T. Watashige, S. Kasahara, Y. Matsuda, and T. Shibauchi, Nematic quantum critical point without magnetism in $FeSe_{1-x}S_x$ superconductors, Proc. Natl. Acad. Sci. U.S.A. **113**, 8139 (2016).

[25] S. Licciardello, J. Buhot, J. Lu, J. Ayres, S. Kasahara, Y. Matsuda, T. Shibauchi, and N. E. Hussey, Electrical resistivity across a nematic quantum critical point, Nature (London) **567**, 213 (2019).

[26] M. Culo, M. Berben, Y. T. Hsu, J. Ayres, R. D. H. Hinlopen, S. Kasahara, Y. Matsuda, T. Shibauchi, and N. E. Hussey, Putative Hall response of the strange metal component in $FeSe_{1-x}S_x$, Phys. Rev. Res. **3**, 023069 (2021).

[27] Y. Sato, S. Kasahara, T. Taniguchi, X. Xing, Y. Kasahara, Y. Tokiwa, Y. Yamakawa, H. Kontani, T. Shibauchi, and Y. Matsuda, Abrupt change of the superconducting gap structure at the nematic critical point in $FeSe_{1-x}S_x$, Proc. Natl. Acad. Sci. U.S.A. **115**, 1227 (2018).

[28] X. Lu *et al.*, Spin-excitation anisotropy in the nematic state of detwinned FeSe, Nat. Phys. **18**, 806 (2022).

[29] C. A. Occhialini, J. J. Sanchez, Q. Song, G. Fabbris, Y. Choi, J.-W. Kim, P. J. Ryan, and R. Comin, Spontaneous orbital polarization in the nematic phase of FeSe, Nat. Mater. **22**, 985 (2023).

[30] L. J. P. Ament, M. van Veenendaal, T. P. Devereaux, J. P. Hill, and J. van den Brink, Resonant inelastic x-ray scattering studies of elementary excitations, Rev. Mod. Phys. **83**, 705 (2011).

[31] C. Jia, K. Wohlfeld, Y. Wang, B. Moritz, and T. P. Devereaux, Using RIXS to uncover elementary charge and spin excitations, Phys. Rev. X **6**, 021020 (2016).

[32] K. Zhou *et al.*, Persistent high-energy spin excitations in iron-pnictide superconductors, Nat. Commun. **4**, 1470 (2013).

[33] J. Pelliciari *et al.*, Reciprocity between local moments and collective magnetic excitations in the phase diagram of $BaFe_2(As_{1-x}P_x)_2$, Commun. Phys. **2**, 139 (2019).

[34] V. Sunko *et al.*, Direct observation of a uniaxial stress-driven Lifshitz transition in Sr_2RuO_4, npj Quantum Mater. **4**, 46 (2019).

[35] See Supplemental Material at http://link.aps.org/supplemental/10.1103/PhysRevLett.132.016501 for detailed data analysis, which includes Refs. [36–38].

[36] M. Bristow, P. Reiss, A. A. Haghighirad, Z. Zajicek, S. J. Singh, T. Wolf, D. Graf, W. Knafo, A. McCollam, and A. I. Coldea, Anomalous high-magnetic field electronic state of the nematic superconductors $FeSe_{1-x}S_x$, Phys. Rev. Res. **2**, 013309 (2020).

[37] B. Pan *et al.*, Two-dimensional digital image correlation for in-plane displacement and strain measurement: A review, Meas. Sci. Technol. **20**, 0620001 (2009).

[38] X. Lu *et al.*, Impact of uniaxial pressure on structural and magnetic phase transitions in electron-doped iron pnictides, Phys. Rev. B **93**, 134519 (2016).

[39] V. N. Strocov *et al.*, High-resolution soft x-ray beamline ADRESS at the Swiss light source for resonant inelastic x-ray scattering and angle-resolved photoelectron spectroscopies, J. Synchrotron Radiat. **17**, 631 (2010).

[40] G. Ghiringhelli *et al.*, SAXES, a high resolution spectrometer for resonant x-ray emission in the 400–1600 eV energy range, Rev. Sci. Instrum. **77**, 113108 (2006).

[41] It is worth noting that these unusual discoveries on strained $x = 0.17$ were first observed in sample 1 and confirmed in sample 2 in a separate RIXS experiment.

[42] M. Chinotti, A. Pal, L. Degiorgi, A. E. Bohmer, and P. C. Canfield, Optical anisotropy in the electronic nematic phase of FeSe, Phys. Rev. B **96**, 121112(R) (2017).

[43] S. Sachdev, *Quantum Phase Transitions* (Cambridge University Press, Cambridge, England, 2007).

[44] A. E. Böhmer, P. Burger, F. Hardy, T. Wolf, P. Schweiss, R. Fromknecht, M. Reinecker, W. Schranz, and C. Meingast, Nematic susceptibility of hole-doped and electron-doped $BaFe_2As_2$ iron-based superconductors from shear modulus measurements, Phys. Rev. Lett. **112**, 047001 (2014).

[45] A. E. Böhmer, T. Arai, F. Hardy, T. Hattori, T. Iye, T. Wolf, H. v. Lohneysen, K. Ishida, and C. Meingast, Origin of the tetragonal-to-orthorhombic phase transition in FeSe: A combined thermodynamic and NMR study of nematicity, Phys. Rev. Lett. **114**, 027001 (2015).

[46] Chiaki Fujii *et al.*, Anisotropic Grüneisen parameter and diverse order parameter fluctuations in iron-based superconductor $Ba(Fe_{1-x}Co_x)_2As_2$, J. Phys. Soc. Jpn. **87**, 074710 (2018).

[47] B. A. Frandsen *et al.*, Local orthorhombicity in the magnetic C_4 phase of the hole-doped iron-arsenide superconductor $Sr_{1-x}Na_xFe_2As_2$, Phys. Rev. Lett. **119**, 187001 (2017).

[48] W. Wang *et al.*, Local orthorhombic lattice distortions in the paramagnetic tetragonal phase of superconducting $NaFe_{1-x}Ni_xAs$, Nat. Commun. **9**, 3128 (2018).

[49] B. A. Frandsen, Q. Wang, S. Wu, J. Zhao, and R. J. Birgeneau, Quantitative characterization of short-range orthorhombic fluctuations in FeSe through pair distribution function analysis, Phys. Rev. B **100**, 020504(R) (2019).

[50] T. Chen *et al.*, Anisotropic spin fluctuations in detwinned FeSe, Nat. Mater. **18**, 709 (2019).

[51] L. Tian, P. Liu, Z. Xu, Y. Li, Z. Lu, H. C. Walker, U. Stuhr, G. Tan, X. Lu, and P. Dai, Spin fluctuation anisotropy as a probe of orbital-selective hole-electron quasiparticle excitations in detwinned $Ba(Fe_{1-x}Co_x)_2As_2$, Phys. Rev. B **100**, 134509 (2019).

[52] A. Wang and C. Petrovic, Electron correlations in the H_{c2} of $Fe_ySe_{1-x}S_x$ ($0.10 \leq x \leq 0.24$, $y \geq 0.9$), Supercond. Sci. Technol. **35**, 115002 (2022).